COUPLED ELECTROMAGNETIC-THERMAL-MECHANICAL SIMULATIONS OF SUPERCONDUCTING RF CAVITIES*

Samuel Posen, Matthias Liepe, and Nicholas Valles
CLASSE, Ithaca, NY 14850, USA

Abstract

The high magnetic and electric radio-frequency fields in superconducting microwave cavities cause heating of the inner cavity surface and generate Lorentz-forces, which deform the shape of the cavity and thereby result in a shift of the fundamental mode frequency. 3-dimensional numerical codes can create complex coupled simulations of the electromagnetic fields excited in a cavity, of heat dissipation and heat transfer, as well as of mechanical effects. In this paper we summarize our simulation results using the engineering simulation package ANSYS [1].

INTRODUCTION

A simulation environment that can couple electromagnetic, mechanical, and thermal analyses with versatile, accessible programming would be an incredibly powerful tool for studying accelerating cavities. This study was meant to evaluate the ability of ANSYS—a popular and widely capable finite element analysis software package—to provide this.

SIMULATIONS

A harmonic electromagnetic analysis of a single-cell Cornell reentrant 1.3 GHz cavity was coupled to a Lorentz force detuning mechanical analysis and a pulsed heating transient thermal analysis. These are just a few examples of what can be accomplished with ANSYS.

Electromagnetic Simulation

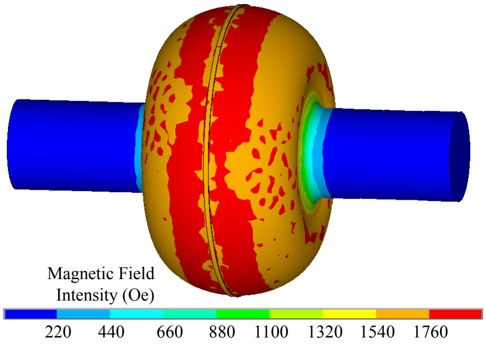

Figure 1: Magnetic field intensity on the cavity surface.

Using the cavity geometry, ANSYS generated a 36459-element mesh, with a conformal 245079-element mesh of the cavity interior. After inputting the surface resistance and port conditions to drive the cavity on resonance with an accelerating voltage of 6 MV, ANSYS calculated the imaginary and real parts of the EM fields inside the cavity. As an example of ANSYS's electromagnetic solver, and to show the fields used to calculate heat flux in the thermal simulations, the magnetic field intensity on the surface of the cavity at 6 MV accelerating voltage is shown in Fig. 1. The thin raised band around the equator in the model is a result of a space left for welding in the geometry file.

Mechanical Simulation

ANSYS derived the radiation pressure from the fields in the cavity interior. This load was transferred to corresponding elements of the cavity itself, and, anchoring the ends, the resulting deformation was calculated, as shown in Fig. 2. Returning the deformed mesh to the electromagnetic solver, the shifted resonant frequency was found, yielding a Lorentz force detuning constant of 0.54 $\frac{Hz}{(MV/m)^2}$.

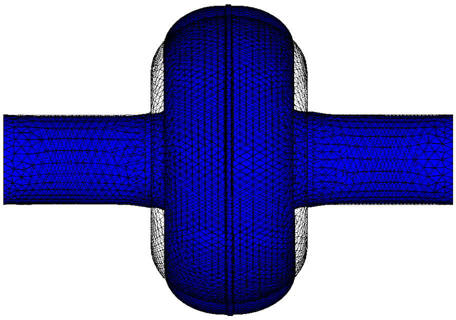

Figure 2: Deformation of cavity with both ends fixed due to radiation pressure. Deflection is exaggerated for visibility.

Thermal Simulation

For this analysis, the transient heating from a high power pulse lasting several hundred µs was examined. A 650 kW pulse was simulated using a heat flux derived from the calculated magnetic fields at each element on the inner surface of the cavity, scaled according to the accelerating voltage. The voltage V at time step k was found from that of the previous step V_{k-1} according to

$$V_k = \left(1 - \frac{\omega_0}{2Q_{L_{k-1}}}\Delta t_s\right) V_{k-1} + \omega\frac{R}{Q}\Delta t_s\sqrt{\frac{2P_f}{\frac{R}{Q}Q_{ext}}} \quad (1)$$

---

* Work supported by the DOE, Grant No. DE-SC0002329.

where Q_L and Q_{ext} are the loaded and external quality factors, ω is the angular driving frequency, ω_0 is the angular resonant cavity frequency, Δt_s is the time interval between steps, P_f is the forward power, and R/Q is the shunt impedance over the quality factor. In this analysis, the cavity was driven on resonance, so $\omega{=}\omega_0$.

After each time step, the temperature and field were compared to the critical temperature and the critical field at that temperature to determine if a given region of the cavity had become normal conducting. The surface resistance for the next step was set accordingly. The surface resistance and magnetic field at each element determined the heat flux to it. The boundary condition on the exterior of the cavity was convective, with coefficient from the Kapitza resistance [2] and a 2 K bath temperature. In order to solve, it was necessary to generate a nonlinear solution that took into account the strongly temperature dependent material properties [3] [4]. The total power dissipated in the walls and the accelerating voltage were used to find the intrinsic cavity quality factor Q_0, which in turn determined the accelerating voltage of the next step by equation 1.

The temperature distribution on one face of the cavity, inside and outside, is shown for various times during the pulse in Fig. 5. The magnetic field on a small area of the cavity surface exceeded the superheating field approximately 109 µs after the start of the pulse. Over the next microseconds, the quench spread, and temperatures in the cavity increased significantly. However, as the Q of the cavity dropped, the fields in the cavity decreased in intensity, so the heat flux decreased, and the cavity began to cool. Some limitations of this preliminary model are evident in these pictures, such as small regions with large temperatures, likely a result of the relatively coarse mesh. The mesh is overlaid to illustrate this effect.

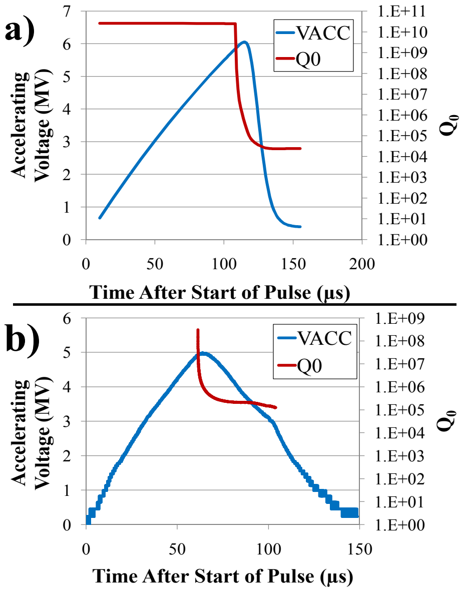

Figure 3: Accelerating voltage and Q_0 of a cavity under pulsed power for a) the ANSYS simulation; b) a real test.

The accelerating voltage and intrinsic Q of the cavity at each time step is plotted in Fig. 3a). At 2 K, the cavity had a Q of 2.6×10^{10}, and it decreased sharply at the quench. The accelerating voltage continued to increase for about 5 µ after the quench initiated, then began to decrease.

This behavior can be compared to that of a real cavity of the same geometry, pulsed at 800 kW in a 2.96 K bath (from [5]). Its response to a pulse is shown in Fig. 3b). The cavity Q drops sharply at about 61 µs, and the accelerating voltage begins to decrease about 3 µs later. The shapes of the plots are very similar to the simulated ones, indicating that the simulation is relevant to the behavior of a real cavity.

The temperature increase as a function of time for one node on the cavity interior and the corresponding node on the exterior is shown in Fig. 4. The higher efficiency of cooling for the outer node can be seen from the lower temperatures at each time, the slower reaction time to a heat flux, and the faster temperature decrease after the quench.

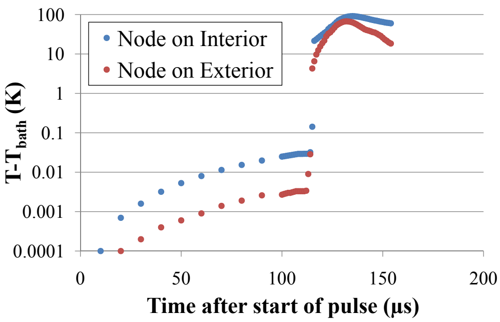

Figure 4: Temperature increase for one node on the cavity interior and the corresponding node on the exterior.

CONCLUSION

ANSYS was used to calculate the harmonic electromagnetic fields and Lorentz force detuning of a Cornell reentrant cavity. It also produced very reasonable results in the first steps towards a complex pulsed heating simulation. The simulation shows good agreement with the behavior of a real cavity under similar conditions. ANSYS shows great promise as a versatile multiphysics simulation environment for accelerating cavities.

REFERENCES

[1] `http://www.ansys.com`.

[2] S. Bousson et al., "Kapitza conductance and thermal conductivity of materials used for SRF cavities fabrication," SRF'99, Santa Fe, 1999, TUP028.

[3] J. Jensen et al., "Brookhaven National Laboratory Selected Cryogenic Data Notebook," Vol. 1, 1980, BNL 100200-R.

[4] T. Schilcher, "Wärmeleitvermögen von niob bei kryogenischen temperaturen," Thesis, 1995, TESLA Report 1995-12.

[5] N. Valles and M. Liepe, "Temperature dependence of the superheating field in niobium," 2010, ArXiv:1002.3182v1.

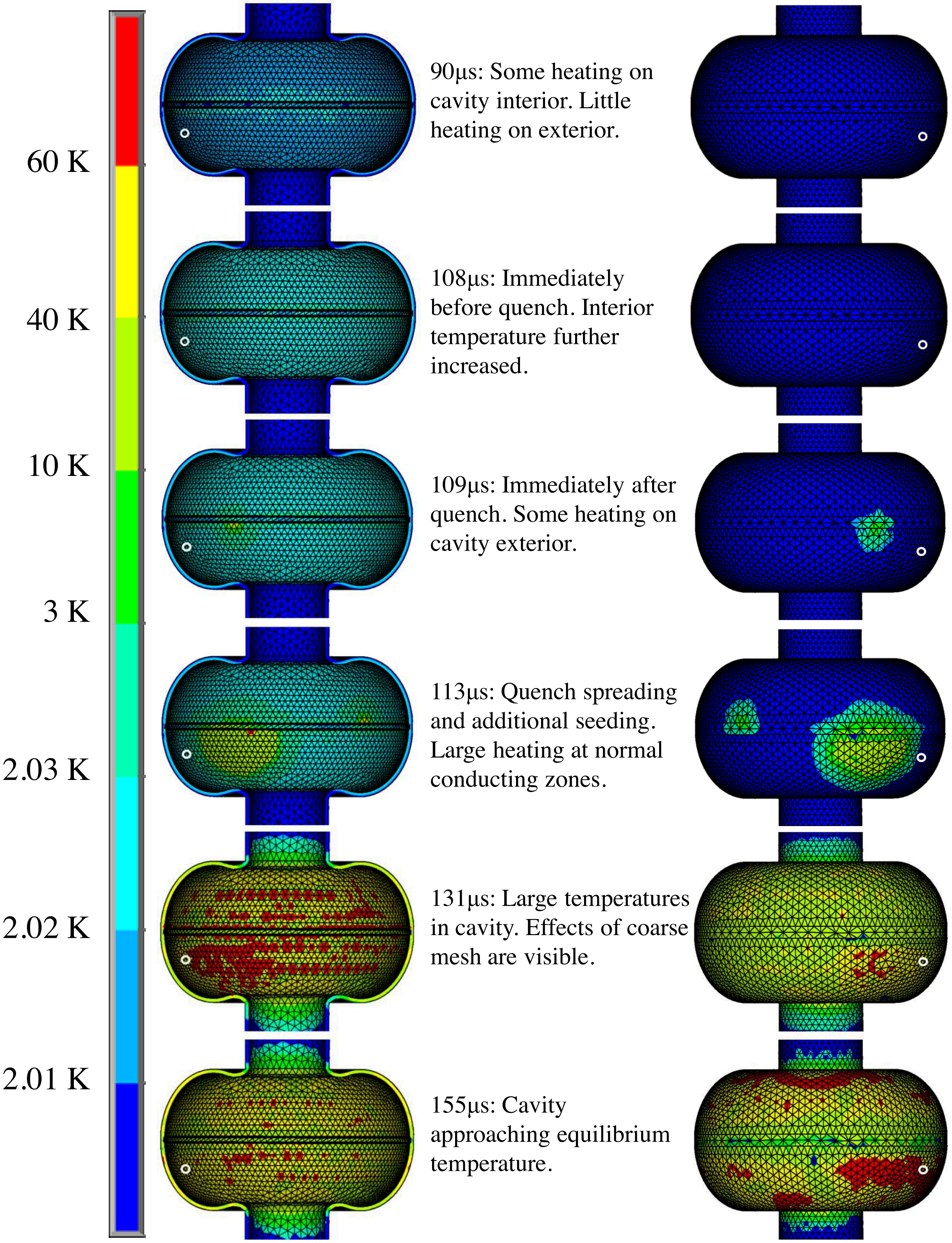

90μs: Some heating on cavity interior. Little heating on exterior.

108μs: Immediately before quench. Interior temperature further increased.

109μs: Immediately after quench. Some heating on cavity exterior.

113μs: Quench spreading and additional seeding. Large heating at normal conducting zones.

131μs: Large temperatures in cavity. Effects of coarse mesh are visible.

155μs: Cavity approaching equilibrium temperature.

Figure 5: Temperature inside (cross section, left) and outside (right) of one face of niobium cavity in a 2 K bath during simulation of 650 kW pulse. Various times after start of pulse are shown. The white circles indicate the locations of the nodes used to create Fig. 4.